RSC Advances

PAPER

View Article Online
View Journal | View Issue

Cite this: *RSC Adv.*, 2026, **16**, 16080

Red-shifting squaraine dyes in the near-infrared region using perimidine heterocycles: synthesis and optical properties

Shahir Sarasiya and Maged Henary *

Received 30th January 2026
Accepted 9th March 2026

DOI: 10.1039/d6ra00833j

rsc.li/rsc-advances

Squaraine dyes are an important class of near-infrared (NIR) probes due to their strong absorption, high molar absorptivity, and structural tunability. However, conventional squaraine dyes employ weak donor units, which suffer from an absorbance maximum in the low 700 nm region. Herein, we report the design, synthesis, and comprehensive characterization of a series of new perimidine-based squaraine dyes that utilize a stronger donor heterocycle to extend optical properties beyond 800 nm. The perimidine donor units were synthesized using a green methodology with high yields. The heterocycles were condensed with squaric acid to afford the squaraine dyes in moderate yields. Optical studies showed strong NIR absorbance, high molar extinction coefficients, and superior photothermal stability. All dyes exhibited low fluorescence. Computational analysis revealed that the facile *E*–*Z* photoisomerization and intramolecular quenching pathways led to low quantum yields. The *Z*-isomer was identified as the global energy minimum.

Introduction

Squaraine dyes have attracted significant interest and development. This is due to their optical properties in the near-infrared region (NIR) and their expansive structural versatility. This has led to numerous reported applications,[1–5] including biomedical,[6,7] photovoltaic,[8,9] biological,[10,11] and environmental sensing,[6,12] for this class of dyes.[1,6,13,14] The NIR region spans from 700 nm to 1700 nm,[15,16] and probes that have optical properties in this region have various applications, as mentioned above, but one of their key uses is as biomedical imaging agents.[17–20] The NIR region is known as the therapeutic window as it offers distinct advantages, specifically minimal absorption by biomolecules and diminished auto-fluorescence, which synergistically enable deeper tissue penetration and heightened sensitivity,[21–23] thus enhancing the signal-to-noise ratio.[24]

Squaraines have shown promising characteristics that make them continually appealing, such as high molar absorptivity, high quantum yields in aqueous media, strong absorbance, and fluorescence in the NIR region.[1,6,25] These characteristics have been attributed to the four-membered ring core. The ring offers structural rigidity to the dye.[26] Squaraine dyes use the four-membered ring because it acts as an acceptor unit, forming a donor–acceptor–donor, D–A–D, system. As the core ring is compact, it allows the electron distribution to be optimal as a good acceptor unit. The electron deficiency of the core allows for the smooth flow of electrons throughout the dye system, maintaining the π-conjugated system. This flow of electrons allows the dye to have NIR absorbance and fluorescence.[1,27,28]

Most squaraine dyes have primarily focused on weaker donor units, such as indole, aniline, and benzothiazole.[1] These scaffolds have shown a lot of promising results, but they have reached an absorbance maximum. The absorbance of the dyes has been capped in the low 700 nm region. This shortcoming has stunted the development of this class of dyes[1–4] because at longer wavelengths in the NIR region, the biological background is significantly reduced, resulting in a better resolution and contrast.[17,29,30] Recent developments have focused on designing squaraine dyes with absorbance maxima deeper in the NIR-I and even the NIR-II region;[20,31,32] however, many avenues for exploration still remain.

Squaraine dyes utilize a DAD system; therefore, to red-shift the absorbance and fluorescence, incorporating a stronger donor unit is a viable tool. A heterocycle that fits these criteria is perimidine. This heterocycle is an ideal candidate because of its conjugated system, large tricyclic size, and optimal electron distribution.[1,33] The perimidine heterocycle is composed of pyrimidine and naphthalene units, and the electron density is shifted to naphthalene, as shown in Fig. 1. Perimidine-based squaraine dyes have been reported previously;[34,35] however, there have been no significant studies on the properties of these dyes.[1]

Herein, we design a series of new perimidine-based squaraine dyes and investigate the photophysical and optical properties of the dyes. Then, we utilize computational analysis to understand the optical properties.

Department of Chemistry, Center of Diagnostics and Therapeutics Georgia State University, Atlanta, GA 30303, USA. E-mail: mhenary1@gsu.edu

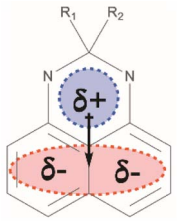

Fig. 1 Perimidine charge distribution.

Experimental

The chemical reagents used in the synthesis were supplied by Fisher Scientific (Fair Lawn, NJ), VWR Int. (Radnor, Pa), Acros Organics (New Jersey), Combi-Blocks (San Diego, CA) and Fisher Chemical (Fair Lawn, NJ). The ^{1}H NMR and ^{13}C NMR spectra were recorded on a Bruker Avance spectrometer (Billerica, MA) and processed using Topspin 4.3.0. The NMR solvent used was chloroform-*d*, 99.8%, or DMSO-d_6, 99.9%, from Cambridge Isotope Laboratory. The UV-Vis spectrophotometer used was the Varian Cary 50 spectrophotometer (Santa Clara, CA). The spectrofluorometer used was the Shimadzu RF-5301 PC spectrofluorometer. The VWR disposable two-sided polystyrene cuvettes with a path length of 1 cm were used for spectroscopic measurements. The quantum yields of dyes were referenced to indocyanine green (ICG). The UV lamp used was a Spectroline (Westbury, New York) model ENF260C, 6000 mW, 254 nm.

Chemistry

Synthesis of the perimidine heterocycles (1–9). In a round-bottom flask, 1 mmol of 1,8-diaminonaphthalene, 1 mmol of the ketone with 10 mol% of squaric acid, and 10 mL of deionized water were added. The solution was heated and stirred at 80 °C. The reaction mixture was heated for 20–120 min, depending on the ketone (Table S1). Once the reaction was completed, the reaction mixture was cooled to room temperature. The product was washed multiple times with deionized water.[36] To reduce the stickiness of the product, an ultrasonic bath was used when washing. If further purification was needed, ethyl acetate/hexane recrystallization was done. The synthesis was confirmed by ^{1}H NMR and melting point analyses.

*2,2-Dimethyl-2,3-dihydro-1H-perimidine (**1**).* Black powder. ^{1}H NMR (400 MHz, $CDCl_3$) δ: 7.26 (q, 2H, J = 7.2 Hz), 7.15 (d, 2H, J = 8.0 Hz), 6.47 (d, 2H, J = 7.2 Hz), 1.507 (s, 6H).

*2,2-Diethyl-2,3-dihydro-1H-perimidine (**2**).* Brown powder. ^{1}H NMR (400 MHz, DMSO-d_6) δ: 7.27 (q, 2H, J = 8 Hz), 7.15 (d, 2H, J = 8.4 Hz), 6.50 (d, 2H, J = 7.2 Hz), 1.77 (q, 4H, J = 7.2 Hz), 0.99 (t, 6H, J = 7.6 Hz).

*2-Isopropyl-2-methyl-2,3-dihydro-1H-perimidine (**3**).* Violet viscous liquid. ^{1}H NMR (400 MHz, $CDCl_3$) δ: 7.22 (t, 3H, J = 8.0 Hz), 7.11 (d, 2H, J = 8.4 Hz), 6.45 (d, 2H, J = 7.2 Hz), 4.32 (s, 2H), 2.09 (m, 1H), 1.361 (s, 3H), 1.03 (d, 6H, J = 24.8 Hz).

*1′H,3′H-Spiro[cyclopentane-1,2′-perimidine] (**4**).* Brown powder. ^{1}H NMR (400 MHz, $CDCl_3$) δ: 7.25 (d, 4H, J = 12.8 Hz), 6.53 (s, 2H), 4.28 (s, 2H), 1.83 (d, 8H, J = 12.2 Hz).

*1′H,3′H-Spiro[cyclohexane-1,2′-perimidine] (**5**).* Brown powder. ^{1}H NMR (400 MHz, $CDCl_3$) δ: 7.27 (q, 2H, J = 12 Hz), 7.17 (d, 2H, J = 8.0 Hz), 6.52 (d, 2H, J = 7.2 Hz), 4.36 (s, 2H), 1.77 (d, 4H, J = 6 Hz), 1.63 (q, 4H, J = 8.2 Hz), 1.54 (d, 4H, J = 4.8 Hz).

*2-Methyl-2-phenyl-2,3-dihydro-1H-perimidine (**6**).* Brown viscous liquid. ^{1}H NMR (400 MHz, $CDCl_3$) δ: 7.58 (d, 2H, J = 7.6 Hz), 7.23 (q, 4H, J = 9.6 Hz), 7.13 (t, 3H, J = 11.2 Hz), 6.53 (d, 2H, J = 7.2 Hz).

*2-(2-Methyl-2,3-dihydro-1H-perimidin-2-yl)phenol (**7**).* Orange-brown viscous liquid. ^{1}H NMR (400 MHz, $CDCl_3$) δ: 12.20 (s, 1H), 7.74 (d, 1H, J = 8.0 Hz), 7.47 (t, 1H, J = 15.6 Hz), 7.18 (m, 2H), 7.15 (d, 2H, J = 8.0 Hz), 6.99 (d, 1H, J = 8.4 Hz), 6.90 (t, 1H, J = 15.6 Hz), 6.47 (d, 2H, J = 7.2 Hz), 4.30 (s, 1H), 2.63 (s, 3H).

*4-(2-Methyl-2,3-dihydro-1H-perimidin-2-yl)phenol (**8**).* Brown viscous liquid. ^{1}H NMR (400 MHz, DMSO-d_6) δ: 7.37 (d, 2H, J = 4.4 Hz), 7.09 (t, 2H, J = 4.0 Hz), 6.82 (d, 2H, J = 4.4 Hz), 6.58 (d, 2H, J = 4.4 Hz), 6.47 (d, 2H, J = 4 Hz), 1.60 (s, 3H).

*2-(4-Chlorophenyl)-2-methyl-2,3-dihydro-1H-perimidine (**9**).* Orange-brown viscous liquid. ^{1}H NMR (400 MHz, $CDCl_3$) δ: 7.90 (d, 2H, J = 8.4 Hz), 7.48 (d, 1H, J = 8.0 Hz), 7.44 (d, 2H, J = 8.4 Hz), 7.23 (m, 2H), 7.15 (m, 2H), 6.51 (d, 1H, J = 9.2 Hz), 6.47 (d, 1H, J = 7.2 Hz), 4.18 (s, 2H), 1.51 (s, 3H).

Synthesis of the perimidine-based squaraine dyes (SQ1–9). In a round-bottom flask, 1 mmol of the perimidine heterocycle and 0.5 mmol of squaric acid were added in a 2 : 1 mixture of butanol and toluene. A Dean–Stark apparatus was used to capture water in the condensation reaction. The reaction mixture was refluxed for 3 h and was monitored using TLC and UV-Vis spectroscopy. Once the reaction was completed, the solution was cooled to room temperature. The reaction mixture was washed with methanol and filtered. The mother liquid was concentrated under reduced pressure. The reduced mother liquid was purified using multiple two-solvent recrystallizations: DCM/hexane, DCM/ethyl acetate and acetone/hexane. If further purification was needed, neutral alumina column chromatography was performed using MeOH/DCM.

*(E)-4-(2,2-Dimethyl-1,2-dihydro-4H-perimidin-3-ium-4-ylidene)-2-(2,2-dimethyl-2,3-dihydro-1H-perimidin-4-yl)-3-oxocyclobut-1-en-1-olate (**SQ1**).* Dark green powder. Yield: 53%. MP: >200 °C. ^{1}H NMR (400 MHz, DMSO-d_6) δ: 7.81 (d, 1H, J = 7.8 Hz), 7.35 (t, 2H, J = 7.6 Hz), 6.81 (t, 2H, J = 9.6 Hz), 6.52 (d, 1H, J = 7.6 Hz), 1.53 (s, 12H). ^{13}C NMR (400 MHz, DMSO-d_6) δ: 183, 149, 145, 136, 134, 132, 129, 124, 118, 115, 110, 109, 109, 66, 28.

*(E)-4-(2,2-Diethyl-1,2-dihydro-4H-perimidin-3-ium-4-ylidene)-2-(2,2-diethyl-2,3-dihydro-1H-perimidin-4-yl)-3-oxocyclobut-1-en-1-olate (**SQ2**).* Dark green powder. Yield: 60%. MP: >200 °C. ^{1}H NMR (400 MHz, DMSO-d_6) δ: 11.22 (s, 1H), 8.43 (d, 1H, J = 8.8 Hz), 7.78 (t, 2H, J = 7.6 Hz), 7.27 (m, 4H), 7.06 (t, 2H, J = 12 Hz), 6.87 (s, 1H), 2.37 (q, 6H), 1.52 (t, 6H, J = 7.6 Hz). ^{13}C NMR (400 MHz, DMSO-d_6) δ: 183, 150, 146, 145, 136, 134, 132, 124, 117, 115, 109, 108, 108, 71, 32, 8.

*(E)-4-(2-Isopropyl-2-methyl-1,2-dihydro-4H-perimidin-3-ium-4-ylidene)-2-(2-isopropyl-2-methyl-2,3-dihydro-1H-perimidin-4-yl)-3-oxocyclobut-1-en-1-olate (**SQ3**).* Green powder. Yield: 65%. MP: >200 °C. ^{1}H NMR (400 MHz, DMSO-d_6) δ: 7.80 (d, 2H, J = 8.4 Hz), 7.32 (q, 2H, J = 8.0 Hz), 6.76 (d, 2H, J = 8.8 Hz), 6.56 (d, 1H,

$J = 7.6$ Hz), 2.10 (s, 1H), 1.458 (s, 1H), 1.02 (q, 6H, $J = 6.4$ Hz). ^{13}C NMR (400 MHz, DMSO-d_6) δ: 183, 150, 145, 137, 134, 129, 124, 118, 116, 115, 110, 109, 109, 71, 35, 23, 17.

*(E)-3-Oxo-2-(1′H,3′H-spiro[cyclopentane-1,2′-perimidin]-4′-yl)-4-(1′H,4′H-spiro[cyclopentane-1,2′-perimidin]-4′-ylidene-3′-ium) cyclobut-1-en-1-olate (**SQ4**).* Dark green powder. Yield: 48%. MP: >200 °C. ^{1}H NMR (400 MHz, DMSO-d_6) δ: 10.69 (s, 2H), 7.8 (d, 2H, $J = 7.8$ Hz), 7.3 (t, 2H, $J = 15.6$ Hz), 6.79 (t, 4H, $J = 14.8$ Hz), 6.54 (d, 2H, $J = 8$ Hz), 1.84 (d, 16H, $J = 7.2$ Hz). ^{13}C NMR (400 MHz, DMSO-d_6) δ: 183, 150, 146, 137, 134, 134, 133, 122, 118, 115, 110, 109, 109, 76, 32, 23.

*(E)-3-Oxo-2-(1′H,3′H-spiro[cyclohexane-1,2′-perimidin]-4′-yl)-4-(1′H,4′H-spiro[cyclohexane-1,2′-perimidin]-4′-ylidene-3′-ium) cyclobut-1-en-1-olate (**SQ5**).* Dark green powder. Yield: 41%. MP: 193–195 °C. ^{1}H NMR (400 MHz, DMSO-d_6) δ: 10.45 (s, 2H), 7.33 (q, 4H, $J = 12.6$ Hz), 6.8 (d, 4H, $J = 9.6$ Hz), 6.592 (s, 2H), 1.655 (s, 20H). ^{13}C NMR (400 MHz, $CDCl_3$) δ: 184, 150, 143, 136, 137, 133, 125, 124, 121, 118, 117, 111, 109, 67, 37, 30, 22.

*(E)-4-(2-Methyl-2-phenyl-1,2-dihydro-4H-perimidin-3-ium-4-ylidene)-2-(2-methyl-2-phenyl-2,3-dihydro-1H-perimidin-4-yl)-3-oxocyclobut-1-en-1-olate (**SQ6**).* Dark purple powder. Yield: 60%. MP: >200 °C. ^{1}H NMR (400 MHz, DMSO-d_6) δ: 11.31 (s, 1H), 8.38 (s, 1H), 7.84 (d, 2H, $J = 8.8$ Hz), 7.6 (d, 2H, $J = 4.8$ Hz), 7.36 (q, 3H, $J = 7.6$ Hz), 7.23 (t, 2H, $J = 6.8$ Hz), 6.82 (d, 2H, $J = 3.2$ Hz), 6.74 (t, 2H, $J = 8$ Hz), 1.875 (s, 3H). ^{13}C NMR (400 MHz, DMSO-d_6) δ: 183, 157, 149, 145, 137, 136, 135, 134, 131, 129, 128, 126, 118, 116, 115, 115, 110, 110, 109, 68, 31.

*(E)-4-(2-(2-Hydroxyphenyl)-2-methyl-1,2-dihydro-4H-perimidin-4-ylidene)-2-(2-(2-hydroxyphenyl)-2-methyl-2,3-dihydro-1H-perimidin-4-yl)-3-oxocyclobut-1-en-1-olate (**SQ7**).* Black powder. Yield: 40%. MP: >200 °C. ^{1}H NMR (400 MHz, DMSO-d_6) δ: 10.58 (s, 3H), 7.81 (d, 3H, $J = 9.2$ Hz), 7.35 (q, 6H, $J = 8.8$ Hz), 6.8 (t, 6H, $J = 10$ Hz), 6.52 (d, 3H, $J = 7.6$ Hz), 1.53 (s, 7H). ^{13}C NMR (400 MHz, DMSO-d_6) δ: 183, 149, 148, 145, 144, 137, 134, 132, 130, 130, 129, 124, 119, 119, 116, 112, 110, 110, 109, 68, 30.

*(E)-4-(2-(4-Hydroxyphenyl)-2-methyl-1,2-dihydro-4H-perimidin-3-ium-4-ylidene)-2-(2-(4-hydroxyphenyl)-2-methyl-2,3-dihydro-1H-perimidin-4-yl)-3-oxocyclobut-1-en-1-olate (**SQ8**).* Green powder. Yield: 45%. MP: >200 °C. ^{1}H NMR (400 MHz, DMSO-d_6) δ: 11.19 (s, 2H), 9.46 (s, 2H), 8.22 (s, 2H), 7.82 (d, 2H, $J = 9.2$ Hz), 7.36 (d, 3H, $J = 7.6$ Hz), 6.80 (t, 3H, $J = 4.8$ Hz), 6.68 (t, 4H, $J = 9.2$ Hz), 1.83 (s, 6 Hz). ^{13}C NMR (400 MHz, DMSO-d_6) δ: 183, 172, 157, 149, 145, 137, 137, 134, 131, 130, 129, 127, 124, 119, 116, 116, 115, 110, 109, 68, 31.

*(E)-4-(2-(4-Chlorophenyl)-2-methyl-1,2-dihydro-4H-perimidin-3-ium-4-ylidene)-2-(2-(4-chlorophenyl)-2-methyl-2,3-dihydro-1H-perimidin-4-yl)-3-oxocyclobut-1-en-1-olate (**SQ9**).* Green powder. Yield: 32%. MP: 195–197 °C. ^{1}H NMR (400 MHz, DMSO-d_6) δ: 10.58 (s, 3H), 7.8 (q, 3H, $J = 15.2$ Hz), 7.42 (d, 3H, $J = 10$ Hz), 7.36 (m, 8H, $J = 20.4$ Hz), 6.82 (t, 2H, $J = 9.2$ Hz), 6.7 (d, 2H, $J = 7.6$ Hz), 1.55 (s, 6H). ^{13}C NMR (400 MHz, DMSO-d_6) δ: 183, 161, 149, 145, 143, 137, 136, 134, 132, 129, 124, 120, 119, 118, 115, 110, 109, 109, 65, 31.

Predicted physicochemical properties. ChemAxon MarvinSketch 23.1.0 (Budapest, Hungary) was used to calculate the log *D* at pH 7.4, rotatable bonds, polarizability, molecular volume, molecular surface area, hydrogen bond donor and acceptor ratio, and total polar surface area for all squaraine dyes.

Optical properties. A 1 mM stock squaraine sample solution was prepared in DMSO. The squaraine sample was weighed on an analytical balance (5-digit) and transferred to an amber glass vial from Fischer Scientific (Pittsburgh, PA, USA), and DMSO was added. The vial was capped and sonicated for 60 min before performing the studies. The absorbance was measured in ethanol (EtOH), dimethyl sulfoxide (DMSO), acetonitrile (ACN) and 50 mM 4-(2-hydroxyethyl)piperazine-1-ethane sulfonic acid (HEPES) buffer. The emission was measured in ethanol (EtOH).

For the absorbance studies, the stock solution of the dyes was diluted to different concentrations (2.0 μM, 4.0 μM, 6.0 μM, 8.0 μM, and 10.0 μM) in EtOH, DMSO and ACN. The concentration range used for HEPES buffer was from 4.0 μM to 14.0 μM. The absorbance maximum values at the maximum wavelength were recorded for the different concentrations and were plotted against the varying concentration in Microsoft Excel to determine the molar extinction coefficient from the slope.

For the fluorescence studies, the stock solution of the different dyes was diluted to 1.20 μM with EtOH. The fluorescence maximum (wavelength) in nanometers was recorded.

Quantum yield. The quantum yield was assessed for the squaraine dyes in EtOH. The quantum yield was compared against a reference dye, indocyanine green (ICG). ICG was used because its absorbance maximum is similar to that of the dyes synthesized and it is an FDA-approved contrasting agent.[37] In the equation, the quantum yield is represented by $\boldsymbol{\Phi}_F$. In the equation, there are denotations of *s* and *x*, where *s* indicates parameters of the reference dye and *x* represents the factors of the synthesized compounds. The *A* term represents the intensity of absorbance at the absorbance maxima, and *F* is the area under the emission curve. *n* represents the refractive index of the solvent; as both ICG and squaraine dyes were measured in ethanol, this parameter cancels out.

$$\boldsymbol{\Phi}_{F,x} = \frac{A_s}{A_x} \times \frac{F_x}{F_s} \times \left(\frac{n_s}{n_x}\right)^2 \times \boldsymbol{\Phi}_{F,s}$$

Photothermal stability. The photothermal stability study was conducted by preparing stock solutions of all the dyes, with ICG used as a reference. Each stock solution was adjusted to an absorbance intensity of 0.8 in 10 mL of ethanol. Two sets of stock solutions were prepared: one exposed to light and the other kept under dark conditions. The dark samples were stored in a drawer at 25 °C without any light exposure, and the containers were wrapped in aluminium foil. The light-exposed samples were kept in a dark enclosed space and irradiated continuously with a 6000-mW, 254-nm UV lamp. The light source was positioned 10 cm away from the samples. Absorbance measurements were recorded at various time intervals of 0 h, 2 h, 4 h, 6 h, 8 h, 10 h, 24 h, 30 h, and 74 h.

Thermal stability. The thermal stability of the dyes was measured using the 1 M stock solution of all dyes and ICG. The samples were prepared by adding a dye concentration so that the absorbance intensity was 0.8 in 50 mM HEPES. The dye

solution's volume was kept to 6 mL and was enclosed in vials (20 mL). The dye-containing vials were placed in an oil bath that was preheated to 50 °C, and the temperature was maintained for 8 h. The absorbance was measured every hour for a total of 8 h.

Computational studies. Spartan 24 V1.2.0 software (Wavefunction Inc., Irvine, CA, USA) was used to perform DFT calculations using the B3LYP level and 6-31G*. HOMO/LUMO energy levels and optimized geometries were generated. The energy profile was prepared using the B3LYP level and 6-31G* for 360 steps. The HOMO–LUMO profile was prepared using the B3LYP level and a 6-31G* for 360 steps.

Results and discussion

Synthesis

The synthesis of the perimidine heterocycles was achieved *via* a reaction between 1,8-diaminonaphthalene and various ketones. This reaction was performed through green chemistry methods, in which water was used as the solvent. In addition, an organocatalyst, squaric acid, was used to accelerate the reaction. Squaric acid acts like an acid and base catalyst.[36] The benefit of using this synthetic pathway, compared to others, was the higher yields (78–99%) and limited use of harsh chemicals, as shown in Scheme 1.

The reaction involving the modified acetophenone took longer to reach completion compared to the aliphatic ketone. The average reaction time for the aliphatic ketone was 28 min, whereas the acetophenone required 79 min (Table 1). The increased reaction time may be attributed to the greater steric bulk of the phenyl ring. In addition, the phenyl-containing perimidine was oilier and stickier than the aliphatic perimidine. As a result, the acetophenone-based perimidines required additional drying to remove water after washing. To speed up the drying of the heterocycle, ethanol or acetone was used to dissolve the compounds, followed by solvent evaporation to remove the excess water.

After forming the perimidine heterocycles, the squaraine dyes were formed using two equivalents of the heterocycle and one equivalence of squaric acid in a butanol and toluene solvent system (Scheme 2). They underwent a condensation reaction to form the perimidine-based squaraine dyes at moderate yields of 32–65%.

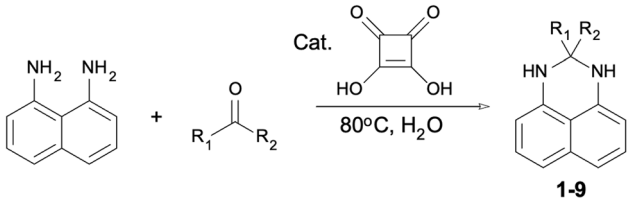

1-9

1: R_1: Me, R_2: Me; **2**: R_1: Et, R_2: Et; **3**: R_1: Me, R_2: iPr; **4**: R_1 & R_2: Cyclopentyl; **5**: R_1: Me & R_2: Cyclohexyl; **6**: R_1: Me, R_2: Phenyl; **7**: R_1: Me, R_2: 2-Hydroxyphenyl; **8**: R_1: Me, R_2: 4-Hydroxyphenyl; **9**: R_1: Me, R_2: 4-Chlorophenyl

Scheme 1 Synthesis of perimidine heterocycles.

Table 1 Reaction (Rxn) time in min and yield and melting point (MP) for each perimidine heterocycle **1–9**

	Ketone	Rxn time	Yield (%)	MP
1		20	90	115–116 °C
2	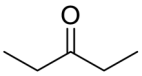	20	90	99–101 °C
3	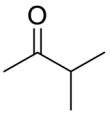	30	85	105–107 °C
4	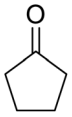	30	85	87–89 °C
5	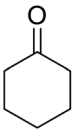	40	85	111–112 °C
6	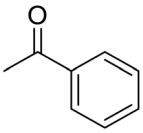	45	93	139–142 °C
7	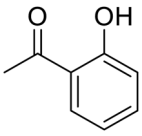	120	78	121–124 °C
8	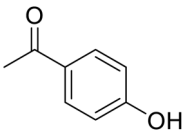	90	82	135–137 °C
9	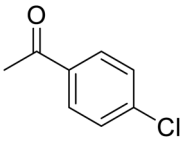	60	85	129–131 °C

Photophysical properties

To evaluate the physicochemical properties of the perimidine-based squaraine dyes, ChemAxon MarvinSketch software was used, as shown in Table S1. The software predicted properties such as distribution coefficient (log *D*), which provides the dyes' ability to disperse in organic and aqueous phases and their hydrophobicity.[38] The most basic perimidine-based squaraine dye, **SQ1**, has a log *D* of 0.65, while further modification, like adding an alkyl chain, **SQ2** and **SQ3**, a cycloalkyl, **SQ4** and **SQ5**, and a phenyl ring, **SQ6–SQ9**, increases the hydrophobicity of the dyes and their log *D* value. The number of rotatable bonds showcases the flexibility and effectiveness of the charge transfer of the molecule. The addition of the noncyclic alkyl chains, **SQ2**

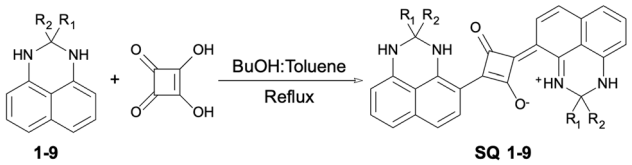

SQ1: R_1: Me, R_2: Me; **SQ2**: R_1: Et, R_2: Et; **SQ3**: R_1: Me, R_2: iPr; **SQ4**: R_1 & R_2: Cyclopentyl; **SQ5**: R_1: Me & R_2: Cyclohexyl; **SQ6**: R_1: Me, R_2: Phenyl; **SQ7**: R_1: Me, R_2: 2-Hydroxyphenyl; **SQ8**: R_1: Me, R_2: 4-Hydroxyphenyl; **SQ9**: R_1: Me, R_2: 4-Chlorophenyl

Scheme 2 Synthesis of perimidine-based squaraine dyes.

and **SQ3**, and the phenyl ring, **SQ6–9**, increases the number of rotatable bonds.

Geometrical analysis of these dyes aims to identify the possible biological applications, and the descriptors identified are the surface area, total polar surface area (TPSA), and volume of the molecule.[39] The addition of the phenyl ring, **SQ6–9**, increases the surface area far more than the alkyl modifications. The TPSA of the core perimidine dye without the addition of any polar group is 90.19, which is due to the multiple nitrogen atoms in the heterocycle. Another descriptor determined for the dyes is the number of hydrogen bond donors (HBDs) and acceptors (HBAs), as they showcase the inter- and intra-molecular interactions. Without the addition of hydrogen bond donor and acceptor groups, the core dye structure has 4 donor sites and 8 acceptor sites. Dye polarizability is an important indicator of how the dye will interact with its surroundings. The trend observed is that as the surface area increases, the polarizability increases as well.

Optical properties

The optical properties of the perimidine-based squaraine dyes were measured in various organic solvents and an aqueous buffer. The solvents used were ethanol, a polar protic organic solvent; DMSO, a polar aprotic organic solvent; and acetonitrile (ACN), a polar aprotic organic solvent. To mimic the body's aqueous environment, HEPES buffer, an aqueous buffer, was utilized. The dyes' optical properties changed with the media due to the solvents' dielectric constant and polarity. FDA-approved indocyanine green (ICG) was used as a reference and a standard for calculating the quantum yield of fluorescence.

The dyes have absorbance maxima that range from 812 nm to 820 nm in ethanol. The slight change in the absorbance is due to the different substituents on the R-groups, as shown in Scheme 2. The absorbance maxima in DMSO are red-shifted, 825 nm to 839 nm, compared to those in ethanol. For squaraine dyes, in DMSO, a slight red-shift is observed compared to ethanol.[25,26,40] By contrast, in ACN, the absorbance of the dyes is blue-shifted, 800 nm to 812 nm, compared to EtOH and DMSO. In 50 mM HEPES buffer, the absorbance band is much broader, and two peaks are observed. The red-shifted peak is observed from 818 nm to 836 nm, while the blue-shifted peak is seen from 752 nm to 768 nm. The intensity of both peaks is about the same, and this can be attributed to aggregation, as shown in Table S2 and Fig. S1–S9. **SQ8** shows the most red-shifted absorbance among all the solvents and media tested.

In the literature, the most commonly used heterocycle for the synthesis of squaraine dyes is the indolium heterocycle.[1] The absorbance of these dyes is typically around 634 nm in ethanol, as shown in Fig. 2, which is at the cusp of the near-infrared (NIR) region. In contrast, perimidine-based squaraine dyes exhibit absorbance maxima above 800 nm, with **SQ1** having an absorbance maximum at 812 nm in ethanol. So, the incorporation of the perimidine heterocycle results in a 178-nm (56 180 cm^{-1}) red-shift in absorbance. This significant bathochromic shift indicates that the perimidine heterocycle is a stronger electron-donating group than indolium.

The fluorescence maximum for the dyes ranges from 821 nm to 827 nm in ethanol. Based on the data, all the synthesized dyes have approximately the same emission wavelength. This indicates that the various modifications do not have a large impact on the fluorescence maximum. So, the emission properties of the probes stem from the core structure, with the R-groups having a limited impact. For the alicyclic-modified dyes, **SQ4** and **SQ5**, the addition of the cyclic ring results in a slight red-shift in emission compared to **SQ1**. This could be due to fewer rotatable bonds. While for the phenyl-modified dyes, further modification of the standard acetophenone group results in a slight blue-shift in emission compared to **SQ1**. The dyes have a small Stokes shift from 5 nm to 9 nm (Table S3 and Fig. S10, S11). In HEPES, the emission band appears as noise.

The molar extinction coefficient for the dyes ranges from 214 843 M^{-1} cm^{-1} to 90 964 M^{-1} cm^{-1} in ethanol. The dyes that have a molar extinction coefficient over 200 000 M^{-1} cm^{-1} are **SQ1** and **SQ3**, and these contain aliphatic chains. However, **SQ4** and **SQ8** have molar extinction coefficients below 100 000 M^{-1} cm^{-1}; apart from these two dyes, the molar extinction coefficient remains high for the other dyes. In DMSO and ACN, the molar extinction coefficient for all the dyes is slightly lower than that in ethanol, ranging between 211 828 M^{-1} cm^{-1} and 83 796 M^{-1} cm^{-1}. However, in the HEPES solution, the molar extinction coefficient is significantly lower, with all the values being less than 63 000 M^{-1} cm^{-1}. This is expected, as the perimidine-based squaraine dyes are hydrophobic in nature, resulting in lower values[6] (Table S4).

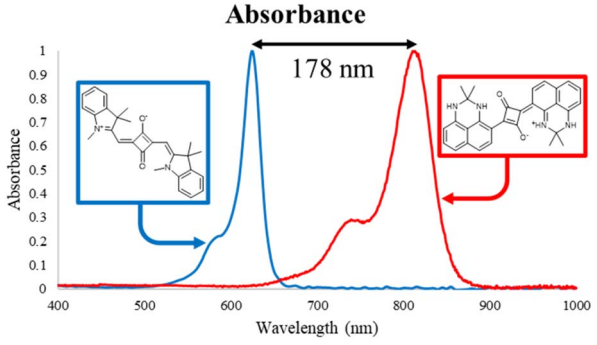

Fig. 2 Normalized absorption of **SQ1** and the indolium-based squaraine dye in ethanol.

The quantum yield for all the squaraine dyes is extremely low, with the values being around 1% for all the dyes, as seen in Table S5. The highest quantum yield is 1.53% for **SQ5**, while the lowest is 0.99% for **SQ1**. These values are much lower than those of the other class of squaraine dyes.[1,6] However, the quantum yield is on par with the few reported perimidine-based squaraine dyes.[1,35] The alicyclic-modified compounds, **SQ4** and **SQ5**, have a slightly higher quantum yield than the other dyes.

Photothermal stability

The photothermal stability of the perimidine-based squaraine dyes was measured. The stability was evaluated under both dark and light conditions, with ICG used as the standard for comparison. Under light conditions after 30 h, ICG had no absorbance, while all the synthesized dyes retained over 31% of their initial absorbance intensity, as shown in Fig. S12. Only at the 72-h point did **SQ3** lose nearly all its absorbance intensity, while the other dyes still exhibited some absorbance intensity. Under dark conditions, all the dyes exhibited high stability compared to ICG (Fig. S13).

The improved photostability of the dyes can be attributed to intramolecular hydrogen bonding between the hydrogen attached to the heterocyclic nitrogen atom and the oxygen atom of the squaraine core. The distance between the nitrogen atoms of the perimidine and the oxygen atom of the squaric acid core ranges from 2.6 to 3.0 Å (Table S6), which falls within the typical range for hydrogen bonding.[41] Previous studies have shown that such intramolecular interactions with the squaraine core enhance the stability of the dye.[18,25]

Thermal stability

To further evaluate the stability of the newly synthesized compounds, thermal stability studies were conducted, as shown in Fig. 3. The dyes were evaluated alongside ICG in the HEPES buffer at 50 °C to understand their stability in an aqueous solution, as the previously reported squaraine dyes had poor aqueous stability.[18,25] The squaraine dyes demonstrated enhanced thermal stability relative to ICG. After 6 h, ICG retained only 12% of its initial absorbance, whereas even the least stable squaraine dye retained 85% of its initial absorbance. These results support the reasoning that intramolecular hydrogen bonding contributes to improved structural rigidity and, consequently, enhanced thermal stability of the dyes.

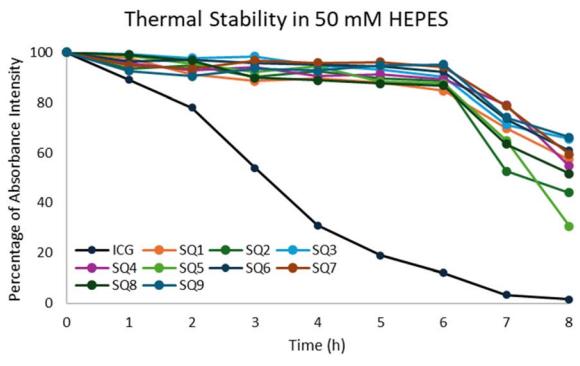

Fig. 3 Thermal stability of **SQ1–9** and ICG. Normalized absorbance over time for the solution in 50 mM HEPES at 50 °C.

Computational analysis

To understand the optical properties, especially the significantly low quantum yield, various computational studies were done using Spartan 24. In the reported literature, squaraine dyes are shown to have high quantum yields.[25] To understand the reasoning behind the opposite results, geometric optimization of the dyes was done, but an interesting result was observed. When the dyes are drawn in the *E*-form, the perimidines are positioned facing the opposite sides, but after optimizing the structure to the *Z*-form, the perimidines are facing the same side and have the lowest energy (Fig. 4). This indicates that the perimidine heterocycle can rotate.[42]

As shown in Fig. 5, there are three points of significance; the highest energy conformer has a perpendicular orientation for the perimidines, where the structure is not planar[43] (Fig. S14). As the planarity is disturbed, this hinders the p-orbital overlapping, limiting the electron flow across the conjugated system, causing this structure to become unstable.[44] When the molecule is in the *E* conformation, the energy is at a local minimum, as depicted in Fig. 5. The energy of this configuration is lower than that in the perpendicular orientation because the *E*-form has a planar structure, allowing for smooth electron flow through the conjugated system. The *Z* configuration is where both heterocycles are positioned in the same spatial orientation, and it is the global minimum. The energy difference between the local and global minima is only 0.0026 a.u., and the difference between the global minimum and highest energy configuration is 0.0421 a.u. (Fig. S15). The slight difference in energy and local and global minima is due to the increase in electrostatic interactions and stronger hydrogen bonding with the negatively charged oxygen group for the *Z* conformer. The distance of nitrogen atom on each heterocycle, closest to oxygen on the squaraine core and the negatively

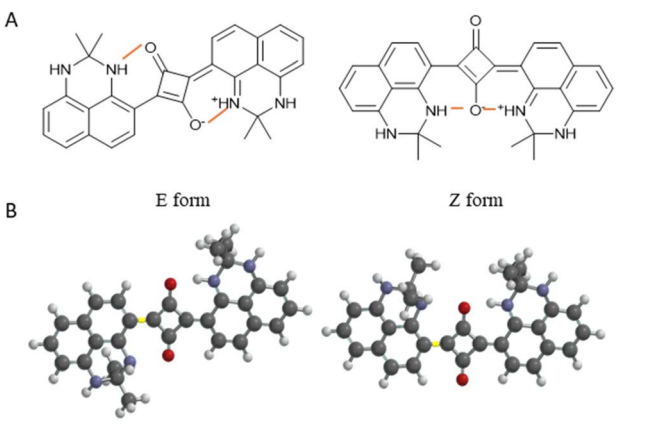

Fig. 4 *E* and *Z* geometric configurations of perimidine-based squaraine dyes for **SQ1**. (A) 2D illustration of the two configurations. (B) 3D representation of the configuration of the dye.

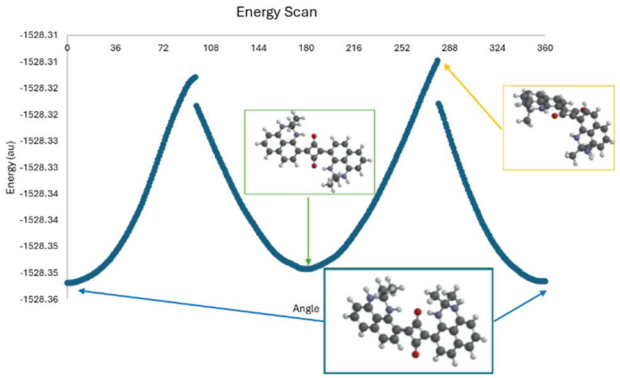

Fig. 5 Energy profile of SQ1, showing the dye configurations at the highest-energy, local-minimum and global-minimum states at various dihedral angles.

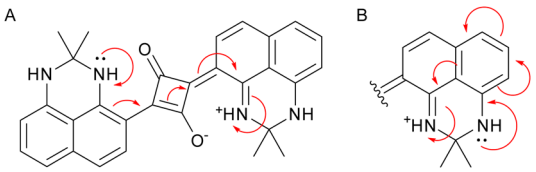

Fig. 6 Electron flow in the (A) perimidine-based squaraine dye and (B) perimidine heterocycle.

oxygen charged, is approximately 3 Å. The distance is within the range for hydrogen bonding, as shown in Table S6.[41]

The energy used to excite the dyes allows for photoisomerization. This is a known pathway to quench fluorescence, as the dye is flexible.[45] Another plausible pathway for the quenching of fluorescence is intramolecular quenching through competing electron flow pathways. The perimidine heterocycle has two nitrogen atoms, which are connected through a conjugated system. So, the lone pair of electrons on the nitrogen atom, that are not part of dye system, can be conjugated to the electron deficent nitrogen in the same heterocycle, Fig. 6. This competing pathway interferes with the electron distribution in the primary dye's conjugate system, resulting in the inactivation of fluorescence.[46]

Conclusions

In summary, nine perimidine-based squaraine dyes are synthesized using a green methodology to form the perimidine heterocycle, followed by a traditional squaraine dye synthesis. The dyes show red-shifted absorbance and emission above 800 nm. The dyes have good molar extinction coefficients and better photothermal stability than ICG. These dyes have very low quantum yields. The dyes showcased photoisomerization, according to computational analysis, where the *Z*-form of the dye is most stable. The unusually low quantum yield of squaraine dyes can be attributed to photoisomerization and intramolecular quenching.

The present work offers a guide for future development of these perimidine-based squaraines for optoacoustic imaging and photothermal/dynamic therapy. This is because optoacoustic imaging and photothermal/dynamic therapy require high non-radiative decay,[47,48] which these dyes provide due to their extremely low quantum yield. In addition, squaraine dyes show electrochemical behaviour.[9,49] In the future, a detailed analysis of the electrochemical properties of the new squaraines will be performed.

Author contributions

S. S., conceptualization, investigation, writing: reviewing and editing; and M. H., conceptualization, funding acquisition, supervising, reviewing, editing, and proofreading the manuscript. All authors have read and agreed to the published version of the manuscript.

Conflicts of interest

There are no conflicts to declare.

Data availability

The data supporting this article have been included as part of the supplementary information (SI). Supplementary information: NMR spectra and further experimental details. See DOI: https://doi.org/10.1039/d6ra00833j.

Acknowledgements

M. H. and S. S. wish to thank the Center for Diagnostics and Therapeutics at Georgia State University for providing S. S. with the CDT fellowship. We acknowledge funding from the National Institutes of Health under grants #R01CA280968B and R01EB034731-01. In addition, M. H. thanks the Brains and Behavior Seed Grant, the Atlanta Clinical and Translational Science Institute for the Healthcare Innovation Program Grant, and the Georgia Research Alliance for the Ventures Phase 1 grant.

Notes and references

1 S. Sarasiya, S. Sarasiya and M. Henary, *Pharmaceuticals*, 2023, **16**, 1299.
2 S. Sreejith, P. Carol, P. Chithra and A. Ajayaghosh, *J. Mater. Chem.*, 2008, **18**, 264–274.
3 A. L. Tatarets, I. A. Fedyunyaeva, E. Terpetschnig and L. D. Patsenker, *Dyes Pigm.*, 2005, **64**, 125–134.
4 E. Terpetschnig and J. R. Lakowicz, *Dyes Pigm.*, 1993, **21**, 227–234.
5 A. Mei, X. He, D. Lei, L. Wang, W. Wang, J. Shao, Q. Shen, F. Jiang and X. Dong, *Coord. Chem. Rev.*, 2025, **527**, 216419.
6 K. Ilina, W. M. MacCuaig, M. Laramie, J. N. Jeouty, L. R. McNally and M. Henary, *Bioconjugate Chem.*, 2019, **31**, 194–213.
7 Ö. Sonkaya, *Turk. J. Chem.*, 2025, **49**, 588–598.
8 G. Chen, H. Sasabe, T. Igarashi, Z. Hong and J. Kido, *J. Mater. Chem. A*, 2015, **3**, 14517–14534.

9 J. Alkabli, *Opt. Mater.*, 2026, **173**, 117860.
10 N. Lange, W. Szlasa, J. Saczko and A. Chwiłkowska, *Pharmaceutics*, 2021, **13**(6), 818.
11 L. Weiss, M. Visser, P. Wagner, A. Augé, O. Florès, N. Pordone, M. Fayolle, P. O. Verhoeven, D. Dziuba and D. Bonnet, *Sens. Diagn.*, 2026, 358–368.
12 S. Thapa, K. R. Singh, S. Gupta, H. N. Lim and S. S. Pandey, *Microchem. J.*, 2025, 116118.
13 X. Wang, Y. Chen, L. Rong, C. Liu, Y. Chen, N. Fu and G. Wang, A Near-Infraed Squaraine Fluorscent Probe for Real-Time Imaging of DNA G-quadruplexes via Disaggregation-Induced Emission in Cancer and Senescence, available at SSRN 6143831, 2026, preprint, DOI: 10.2139/ssrn.6143831.
14 K. B. Ingole, J. Siby, R. Pandya, K. Vanka, K. Krishnamoorthy and J. Nithyanandhan, *Chem.–Asian J.*, 2026, **21**, e70455.
15 F. Zhang and B. Z. Tang, *Chem. Sci.*, 2021, **12**, 3377–3378.
16 K. Shou, C. Qu, Y. Sun, H. Chen, S. Chen, L. Zhang, H. Xu, X. Hong, A. Yu and Z. Cheng, *Adv. Funct. Mater.*, 2017, **27**, 1700995.
17 H. Kang, S. H. Park, G. E. Ozmen, W. Hur, J. Dinh, H. Wang, V. Nguyen, S. Ahn, A. Yamashita, W. R. Stiles, S. Kashiwagi, K. Bao, M. Henary and H. S. Choi, *Chem*, 2025, **11**, 102481.
18 T. Fukuda, S. Yokomizo, S. Casa, H. Monaco, S. Manganiello, H. Wang, X. Lv, A. D. Ulumben, C. Yang and M. W. Kang, *Angew. Chem.*, 2022, **134**, e202117330.
19 H. Li, W. Li, Y. Tang, X. He, Y. Xiong, Y. Gong, J. Lu, X. Pan, J. Wang and N. Hao, *Chem.–Eur. J.*, 2025, e02401.
20 J. Y. Lau, K. Shi, A. G. Oliver and B. D. Smith, *Org. Lett.*, 2025, **27**, 8083–8087.
21 G. Ersoy and M. Henary, *Biomolecules*, 2025, **15**, 119.
22 E. A. Owens, M. Henary, G. El Fakhri and H. S. Choi, *Accounts Chem. Res.*, 2016, **49**, 1731–1740.
23 X. Yang, C. Shi, R. Tong, W. Qian, H. E. Zhau, R. Wang, G. Zhu, J. Cheng, V. W. Yang, T. Cheng, M. Henary, L. Strekowski and L. W. K. Chung, *Clin. Cancer Res.*, 2010, **16**, 2833–2844.
24 Z. M. Essam, G. E. Ozmen, D. Setiawan, R. R. Hamid, R. M. Abd El-Aal, R. Aneja, D. Hamelberg and M. Henary, *Org. Biomol. Chem.*, 2021, **19**, 1835–1846.
25 Y. Yadav, E. Owens, S. Nomura, T. Fukuda, Y. Baek, S. Kashiwagi, H. S. Choi and M. Henary, *J. Med. Chem.*, 2020, **63**, 9436–9445.
26 S. Casa, G. Ersoy Ozmen and M. Henary, *Molbank*, 2023, **2023**, M1576.
27 E. P. Bacher, *Shedding New Light on Squaraines: Utilizing Squaraine Dyes as Effective Tools in Organic Synthesis*, University of Notre Dame, 2020.
28 J. Fan, Z. Wang, H. Zhu and N. Fu, *Sens. Actuators, B*, 2013, **188**, 886–893.
29 H. Kang, M. Shamim, X. Yin, E. Adluru, T. Fukuda, S. Yokomizo, H. Chang, S. H. Park, Y. Cui, A. J. Moy, S. Kashiwagi, M. Henary and H. S. Choi, *Adv. Mater.*, 2022, **34**, 2106500.
30 H. J. Zhou and T. B. Ren, *Chem.–Asian J.*, 2022, **17**, e202200147.
31 H. Gao, Y. Yao, C. Li, J. Zhang, H. Yu, X. Yang, J. Shen, Q. Liu, R. Xu and X. Gao, *Angew. Chem.*, 2024, **136**, e202400372.
32 J. Csucker, E. Didier, J. Pedro Ferreira Assunção, D. Rentsch, R. Kothandaraman, D. Bachmann, I. Shorubalko, F. Nüesch, R. Hany and M. Bauer, *Adv. Sci.*, 2025, 2502320.
33 N. Sahiba and S. Agarwal, *Top. Curr. Chem.*, 2020, **378**, 44.
34 S. Ernst, J. Mistol, B. Senns, L. Hennig and D. Keil, *Dyes Pigm.*, 2018, **154**, 216–228.
35 K. Umezawa, D. Citterio and K. Suzuki, *Chem. Lett.*, 2007, **36**, 1424–1425.
36 S. Khopkar and G. Shankarling, *J. Chem. Sci.*, 2020, **132**, 31.
37 H. S. Choi, K. Nasr, S. Alyabyev, D. Feith, J. H. Lee, S. H. Kim, Y. Ashitate, H. Hyun, G. Patonay, L. Strekowski, M. Henary and J. V. Frangioni, *Angew. Chem., Int. Ed.*, 2011, **50**, 6258–6263.
38 T. E. Ahmed and M. Henary, *Org. Lett.*, 2025, **27**, 6623–6629.
39 R. Pirie, H. A. Stanway-Gordon, H. L. Stewart, K. L. Wilson, S. Patton, J. Tyerman, D. J. Cole, K. Fowler and M. J. Waring, *RSC Med. Chem.*, 2024, **15**, 3125–3132.
40 D. dos Santos Pisoni, M. L. d. C. Zanirati, L. H. Lapazin, B. B. de Araújo, F. S. Rodembusch, L. F. Campo and F. L. Coelho, *New J. Chem.*, 2025, **49**, 17515–17524.
41 J. M. MacLeod and F. Rosei, in *Comprehensive Nanoscience and Technology*, ed. D. L. Andrews, G. D. Scholes and G. P. Wiederrecht, Academic Press, Amsterdam, 2011, pp. 13–68, DOI: 10.1016/B978-0-12-374396-1.00098-2.
42 T. Oka, T. Maeda, D. Sakamaki, N. Suzuki, S. Yagi, S. Kodama and H. Fujiwara, *Org. Chem. Front.*, 2025, **12**, 42–47.
43 F. Dietz and S. K. Rentsch, *Chem. Phys.*, 1985, **96**, 145–151.
44 J. M. Marin-Beloqui, S. Gómez, H. I. Gonev, M. Comí, M. Al-Hashimi and T. M. Clarke, *Chem. Sci.*, 2023, **14**, 812–821.
45 V. Y. Artyukhov and E. I. Sinchenko, *Russ. Phys. J.*, 2001, **44**, 718–722.
46 S. Yokomizo, M. Henary, E. R. Buabeng, T. Fukuda, H. Monaco, Y. Baek, S. Manganiello, H. Wang, J. Kubota and A. D. Ulumben, *Adv. Sci.*, 2022, **9**, 2201416.
47 M. D. Laramie, M. K. Smith, F. Marmarchi, L. R. McNally and M. Henary, *Molecules*, 2018, **23**, 2766.
48 A. St. Lorenz, E. R. Buabeng, O. Taratula, O. Taratula and M. Henary, *J. Med. Chem.*, 2021, **64**, 8798–8805.
49 A. S. Al Zbedy and S. A. Al-horaibi, *J. Mol. Struct.*, 2025, 144638.